UDK 666.798.2:519.61/.64
Original scientific article/Izvirni znanstveni članek

ISSN 1580-2949
MTAEC9, 48(6)861(2014)

# MODELLING OF OPERATING PARAMETERS IN AN SOFC TESTING SYSTEM

## MODELIRANJE IN PARAMETRI DELOVANJA SISTEMA ZA PREIZKUŠANJE SOFC

**Tina Skalar[1,2], Marjan Marinšek[1,2], Martin Lubej[1], Marjan Lukežič[1,2], Tomaž Skalar[3], Jadran Maček[1,2]**

[1]University of Ljubljana, Faculty of Chemistry and Chemical Technology, Aškerčeva 5, 1000 Ljubljana, Slovenia
[2]Center of Excellence Low-Carbon Technologies (CO NOT), Hajdrihova 19, 1000 Ljubljana, Slovenia
[3]School Centre of Ljubljana, Mechanical and Chemical High School, Aškerčeva 1, 1000 Ljubljana, Slovenia
tina.skalar@fkkt.uni-lj.si

*Prejem rokopisa – received: 2013-10-04; sprejem za objavo – accepted for publication: 2014-01-02*

High-temperature solid-oxide fuel cells (SOFCs) are assembled from three solid components: electrolyte, anode and cathode. In this work, samarium-doped ceria (SDC) was used as the electrolyte material. Due to their similar temperature-expansion coefficients, Ni-SDC cermet was used as the anode while Pt was used as the cathode.
The aim of this work was to study the materials' responses under operating conditions in the testing set-up. The temperature gradients generated within the SOFC testing may cause high stresses in the materials, which eventually lead to a delamination of a layered structure. Since an accurate temperature control in several points of the multilayer SOFC system is rather difficult or even impossible to achieve, a model of mass and energy balances was written and subsequently solved with the method of finite elements in two dimensions. The results of the mathematical modelling during the warm-up, steady-state or cool-down periods were used to profile the temperatures within the testing SOFC set-up and to predict the dimensional changes of individual layers in the SOFC multilayer structure. The influence of the temperature gradients was also studied experimentally.
Based on the modelling results, an optimization of the operating conditions was proposed in order to reduce the thermal stresses built in the materials.

Keywords: Ni-SDC, SOFC, modelling, temperature gradient, thermal stress, optimization

Visokotemperaturne gorivne celice s trdnimi oksidi (SOFC) so sestavljene iz treh trdnih komponent: elektrolita, anode in katode. V tem delu je bil kot elektrolitni material uporabljen cerij, dopiran s samarijem (SDC). Zaradi podobnih koeficientov toplotnega raztezka je bil kot anoda uporabljen Ni-SDC-kermet, kot katoda pa Pt.
Namen tega dela je bil študij vedenja materialov med delovnimi razmerami v preizkusnem sestavu. Temperaturni gradient, ki se pojavi pri preizkušanju SOFC, lahko povzroči velike napetosti v materialih, kar lahko povzroči razslojevanje plastne strukture. Ker je težko oziroma nemogoče kontrolirati temperature v več točkah večplastnega sistema SOFC, je bil napisan model uravnoteženja mase in energije, ki je bil narejen z uporabo metode končnih elementov v dveh dimenzijah. Rezultati matematičnega modela so bili uporabljeni za izdelavo profila temperature med ogrevanjem, delovanjem in ohlajanjem SOFC-sistema in za napovedovanje dimenzijskih sprememb posameznih plasti v večplastni zgradbi tega sistema. Vpliv gradientov temperature je bil preučevan tudi eksperimentalno.
Na podlagi rezultatov modeliranja je bila za zmanjšanje toplotnih napetosti v materialih predlagana optimizacija delovnih razmer.

Ključne besede: Ni-SDC, SOFC, modeliranje, gradient temperature, toplotna napetost, optimizacija

## 1 INTRODUCTION

Solid-oxide fuel cells (SOFCs) are devices that convert chemical energy into electrical energy. They have a high efficiency of energy conversion and low pollutant emission, low cost and flexibility in the choice of fuels.[1–5] An operating SOFC consists of an anode, an electrolyte and a cathode. Recently, SDC (samaria-doped ceria) has been used as the electrolyte in IT-SOFC (intermediate-temperature solid-oxide fuel cells). SDC is an advanced ceramic well-known for its high oxygen ionic conductivity compared to the conventional electrolyte, YSZ, at the operating temperatures of IT-SOFC (400–700 °C).[6–11] The main reasons for the selection of Ni-SDC as the anode material are its relatively good ionic and electronic conductivity, acceptable catalytic activity for hydrogen or hydro-carbon oxidation, and its thermal-expansion coefficient (TEC), which is compatible with the SDC electrolyte.[12–15] The TEC of the anode cermet is higher than the TEC of the electrolyte. The differences in the thermal-expansion coefficients of the components may cause a residual stress in the anode or/and electrolyte layer and, consequently, a SOFC stack delamination. From this perspective, the reliability is seriously dependant on the thermal stress. The residual stresses in SOFC were investigated both experimentally and theoretically.[16–20]

A theoretical analysis of the residual stress may be modelled with the finite-element method (FEM).[21–23] The FEM allows a transformation of a continuous problem into a discrete problem with a finite number of degrees of freedom. Such an approach has already been used by several authors, in whose works the parameters can be arbitrarily changed,[16,24,25] yielding fast and economical results that can be immediately evaluated.

For this reason, a new SOFC testing system was developed. The system allows quick changes of the operating conditions (temperature, atmospheres). The significance of this work is the ability to determine the optimum operating parameters at which the SOFC multilayer membrane is not exposed to the critical thermal stress caused by temperature gradients.

## 2 EXPERIMENTAL PROCEDURE

### *2.1 Material preparation*

The electrolyte samaria-doped ceria (SDC) and anode nickel-oxide samaria-doped ceria (NiO-SDC) were synthesized using metal acetates and ethylene glycol.[26,27] The final crystalline products were calcined to the final mixture of metal oxides. The electrolyte powder was pressed into a tablet and pre-sintered at 1000 °C in air in order to prepare a dense body and to ensure the mechanical strength for the anode printing. The anode was screen printed (the final thickness 20 μm) on the electrolyte. Such a bilayer system was co-sintered at 1250 °C to form a good contact between both layers. After co-sintering, the electrolyte reaches 93 % of its relative density and it is thick 3 mm. On the opposite side of the electrolyte, platinum as the cathode was sputtered in a thickness of 50 nm.

### *2.2 Testing system*

The testing system (**Figure 1**) consists of a multilayer tablet (anode-electrolyte-cathode) (3), sealed in steatite ceramics (9). The platinum electrical contacts (1) are pressed against the anode and cathode sides of the membrane. On both sides of the steatite, double quartz glass (8) is added to prevent mixing the inner and outdoor atmospheres, and to prevent mixing between the oxidative and reductive atmospheres (Viton o-rings (7) are used for sealing). $\alpha$-alumina wool (2-cm thick) (2) is used to insulate the system. Heating plugs (Hidria) (6) are embedded into a stainless-steel (1.4404) case (4) and fixed to the construction with four screws. The testing system is isolated with $\alpha$-alumina insulation 2 cm (2). The thermocouple NiCr-Ni (5) is pushed through a small hole and coupled with the display.

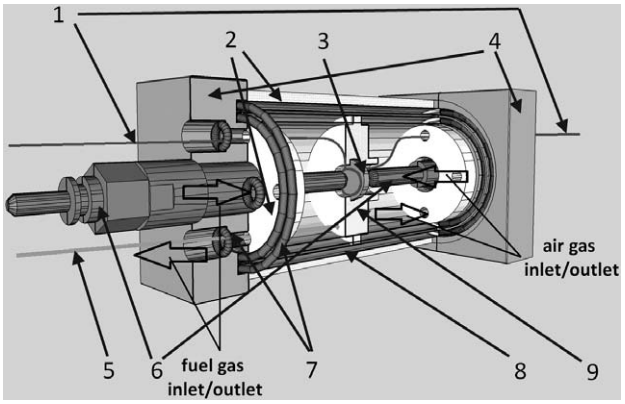


**Figure 1:** Configuration of the testing cell
**Slika 1:** Sestava preizkusnega sistema za SOFC

### *2.3 Model*

#### *2.3.1 Velocity and the temperature profile*

The gas flow and temperature distribution were simulated using the numerical methods. The transport of mass and energy was calculated by following the continuum theory, which utilizes the following differential equations (Eq. 1, 2, 3):

$$\rho \frac{\partial \vec{v}}{\partial t} = -\nabla p - \vec{v} \cdot \nabla \vec{v} + \mu \nabla^2 \vec{v} + \rho \vec{g} \tag{1}$$

$$\frac{\partial \rho}{\partial t} = -\nabla \cdot (\rho \vec{v}) \tag{2}$$

$$\rho c_p \frac{\partial T}{\partial t} = -\rho c_p \vec{v} \cdot \nabla T + \nabla \cdot (k \nabla T) + Q \tag{3}$$

where $\rho$ stands for the fluid density, $k$ stands for the fluids' thermal conductivity and $c_p$ is the fluids' thermal capacity. Since the radiation is not negligible at such high temperatures, it was considered as a heat source at the cell walls, which are not transparent. The radiation-heat source was defined as (Eq. 4, 5):

$$-\vec{n}(-k \nabla T) = \varepsilon (G - \sigma T^4) \tag{4}$$

$$(1 - \varepsilon) G = J_0 - \varepsilon \sigma T^4 \tag{5}$$

The heat is introduced as a homogeneous-volume heat source at the glow plug. The heat is dissipated at the outer boundaries with the heat flux corresponding to the wall temperature (Eq. 6) and the heat-transfer coefficient obtained with the Churchill and Chu correlation (Eq. 7):

$$\vec{q} = \bar{h} (T - T_\infty) \tag{6}$$

$$Nu = \left( 0.825 + \frac{0.387 Ra^{1/6}}{(1 + (0.492 / Pr)^{9/16})^{8/27}} \right) \tag{7}$$

where $\bar{h}$ is the mean heat-transfer coefficient, $T_\infty$ is the surrounding temperature, $Ra$ is the Rayleigh number and $Pr$ is the Prandtl number of the surrounding air.

The system of differential equations was solved utilizing the finite-element method in a 2D axisymmetric geometry; the stationary state was achieved at the 35$^{th}$ iteration.

#### *2.3.2 Mechanical stress*

The mechanical stresses inside the electrolyte and anode were calculated using a linear elastic-material model (Eq. 8, 9) in combination with the thermal expansion (Eq. 10):

$$-\nabla \cdot \sigma = \vec{F}_v \tag{8}$$

$$\varepsilon = \frac{1}{2} \left( (\nabla \vec{v})^T - \nabla \vec{v} \right) \tag{9}$$

$$\sigma - \sigma_0 = C : (\varepsilon - \alpha (T - T_0) - \varepsilon_0) \tag{10}$$

where $\sigma$ is the stress tensor, $\vec{F}_v$ is the force, $\varepsilon$ stands for the general strain, $\alpha$ is the linear thermal-expansion coefficient and $T_0$ is the reference temperature. The reference temperature was defined as the temperature when there is no stress in the material.

The mechanical model was solved utilizing the finite elements in the 2D axisymmetric geometry.

For all the materials the average emissivity ($\varepsilon$) of 0.8 was used. Young's modulus ($E$), Poisson ratio ($\nu$), the density ($\rho$) and the thermal-expansion coefficient ($\alpha$) were $200 \cdot 10^9$ Pa [24], 0.32 [24], 7600 kg/m$^3$, $11.5 \cdot 10^{-6}$ K$^{-1}$ [28] and $55 \cdot 10^9$ Pa [24], 0.17 [29], 8900 kg/m$^3$, $13 \cdot 10^{-6}$ K$^{-1}$ [24] for SDC and NiO-SDC, respectively. The densities for both materials were calculated as the Archimedes' densities from the dimensions of the sintered bodies.

## 3 RESULTS AND DISCUSSION

The main advantage of the developed SOFC testing system is its rather simple design, assembled from a relatively small number of parts and easy to manipulate. Such a simplified SOFC design allows a quick assembly or dismantling of the system and makes it possible to start a new testing cycle in literally a matter of minutes. Furthermore, the relative positions of the heating elements close to the SOFC membrane heat up the membrane multilayer tested element and both inner chambers of the testing system rather quickly. The prompt temperature response of the SOFC testing element further makes the testing cycles much shorter. However, it is well known that a rapid temperature change in a ceramic multilayer system, in which individual layers exhibit different temperature-expansion coefficients, builds stresses and may initiate a crack formation, which eventually cause a complete system delamination. To avoid such an unwanted multilayer degradation, numerous tests are required in order to determine the temperature regime during a testing cycle. Due to the time-consuming submission of many testing membranes to various heating or cooling rates, we chose an alternative way of the system testing: employing a mathematical simulation model and predicting the temperature gradients as well as the stress fields built in the tested membrane.

A closer insight into the operating of the testing system in a steady state (including the tested membrane) is presented in **Figure 2**. Due to the relative positions of the heating elements, the temperature distributions in the two chambers are not identical (**Figure 2a**). The anode side of the tested membrane is at somewhat lower temperatures creating a temperature gradient across the multilayer membrane. An additional temperature gradient at any horizontal plane is caused by the fact that the membrane centre is at a higher temperature than its outer ring (**Figure 2d**). The maximum temperature differences across the membrane or along its diameter are 15 °C and 55 °C, respectively. To roughly verify the modelled temperature fields in both SOFC chambers, additional temperature measurements using a NiCr-Ni thermocouple were conducted. The measuring points are marked in **Figure 2b**. According to the temperature measurements, the mathematical model used describes the stationary conditions in the tested system rather well (**Table 1**). The temperature mismatches between the modelled and measured temperatures in either point did not exceed 7 °C. The mathematical modelling additionally revealed that the temperature field inside both of the SOFC chambers is negligibly influenced by the introduction of fresh cold gas (**Figure 2b**). The gas entering the SOFC chamber is almost instantly heated up to the chamber temperature due to a relatively low inlet gas flow (≈ 15 mL/min)

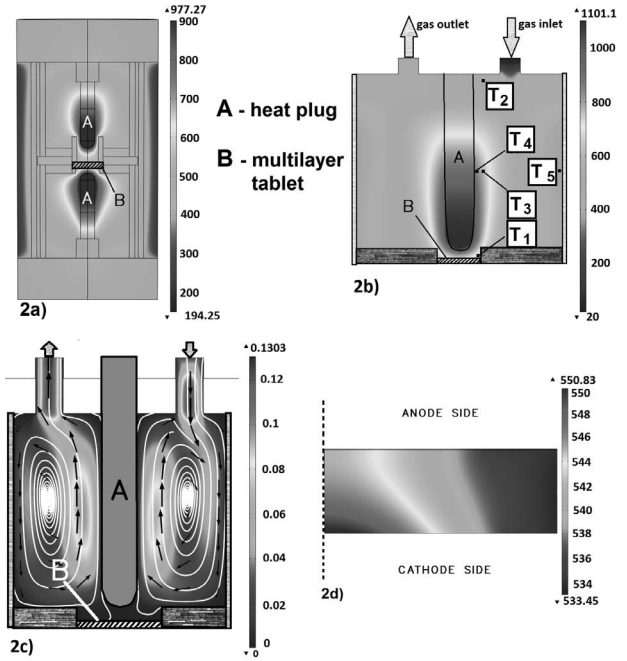


**Figure 2:** a) Temperature distribution in the inner chambers of the SOFC testing system, b) temperature distribution on a plane through the anode inner chamber and the positions of the temperature control, c) fluid-velocity simulation together with the gas trajectories in the anode inner chamber and d) temperature distribution on a plane through the tested membrane (only one half of the membrane cross-section is presented)

**Slika 2:** a) Porazdelitev temperature po preizkusnem sistemu za SOFC, b) porazdelitev temperature po anodnem prostoru preizkusne celice z vrisanimi točkami, kjer smo merili temperature s termoelementom in jih primerjali z modelirano vrednostjo, c) simulacija hitrosti in smeri gibanja fluida po anodnem prostoru in d) porazdelitev temperature po preizkusni membrani (prikazana je le polovica membrane)

**Table 1:** Comparison between the modelled and measured temperatures in the testing system at stationary operating conditions

**Tabela 1:** Primerjava modeliranih in izmerjenih temperatur v sistemu pri stacionarnih razmerah obratovanja

| Measuring point | $T_{modelled}$ /°C | $T_{measured}$ /°C |
|---|---|---|
| 1 | 539 | 536 |
| 2 | 537 | 532 |
| 3 | 737 | 730 |
| 4 | 782 | 776 |
| 5 | 495 | 493 |

and a relatively large chamber volume. This fact is not surprising since only ≈ 72 W is needed to heat a gas flow of 15 mL/min from room temperature to the chamber temperature. The fresh-gas inlet together with the created temperature gradient is the cause of the gas turbulence in the SOFC chamber. The gas velocity is the highest close to the heating element and relatively low near the surface of the tested membrane (**Figure 2c**). The complex movement path of gas molecules is indicated by their trajectories. Despite the lowest gas velocity being near the membrane surface (≈ 0.02 m/s), no gas pockets with stationary atmosphere could be observed. The dynamic atmospheric condition at the membrane surface is important from the practical perspective of the SOFC. Only dynamic conditions may deliver fresh reactants to the diffusion layer of the porous membrane catalyst and remove the gaseous products.

One of the major problems of planar SOFC systems is their reliability. The residual stresses, which mainly arise from the different thermal-expansion coefficients of the components, may destroy the SOFC structure during the temperature alteration. The first critical point in the SOFC membrane preparation path is the cooling of the multilayer system after its sintering and the subsequent reduction of NiO to Ni. Specifically, the thermal stresses in the multilayer system start to build up below the plastic-deformation temperature, i.e., the sintering temperature. From this perspective, it could be assumed that the system is stress-free at the sintering temperature and can be submitted to the highest stresses at room temperature.[29] These build-up stresses may be as high as several hundred MPa and may cause cracks to the form. The residual stresses after the membrane sintering are relatively difficult to measure. However, by adopting an appropriate mathematical model, the induced stresses in the multilayer system can be calculated quite easily. In the testing, the stress-free state was adopted at 1250 °C where the NiO/SDC anode material and the SDC electrolyte were co-sintered. The subsequent reduction of NiO to Ni should not induce an additional stress since Ni may undergo plastic deformation. Similarly, the sputtered Pt cathode (50 nm) can also be easily plastically deformed and, thus, it does not contribute to any stress formation. For this reason, the thin cathode layer was omitted from further mathematical modelling.

Based on various shrinkages of the Ni-SDC and SDC layers during cooling, the modelled residual thermal stress at room temperature is shown in **Figure 3**. Due to the higher thermal-expansion coefficient, the Ni-SDC layer tends to shrink more than the SDC electrolyte. In a hypothetical situation in which both layers subjected to an uneven material shrinkage have approximately the same thickness, the induced stress should bend the bilayer system where the layer with the smaller shrinkage (SDC) forms a convex outer surface. In the investigated bilayer system, the SDC electrolyte thickness is 3 mm, while the Ni-SDC anode thickness is only 20 μm. As a consequence, the system bending is negligible, owing to the rather thin Ni-SDC layer. Nevertheless, rather high stress fields are created at room temperature. The absolute stress values are highest in the Ni-SDC anode layer (≈ 130 MPa) close to the anode-electrolyte

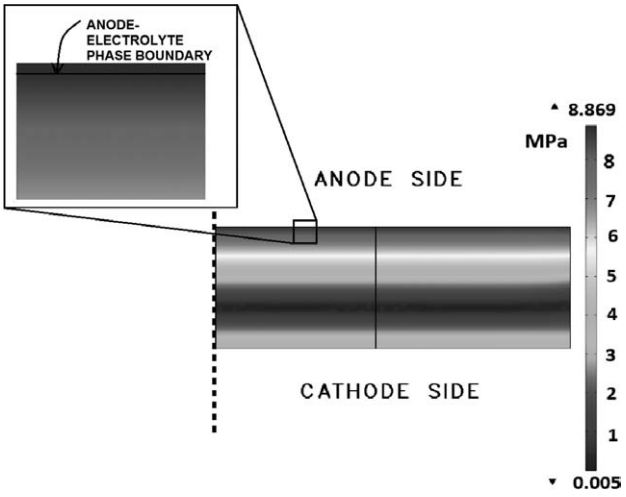


**Figure 3:** Simulated residual thermal stress in the cross-section of bilayer system NiO/SDC-SDC at room temperature (only one half of the membrane cross-section is presented)

**Slika 3:** Simulacija zaostalih toplotnih napetosti v dvoplastnem sistemu NiO/SDC-SDC pri sobni temperaturi (prikazana je le polovica membrane)

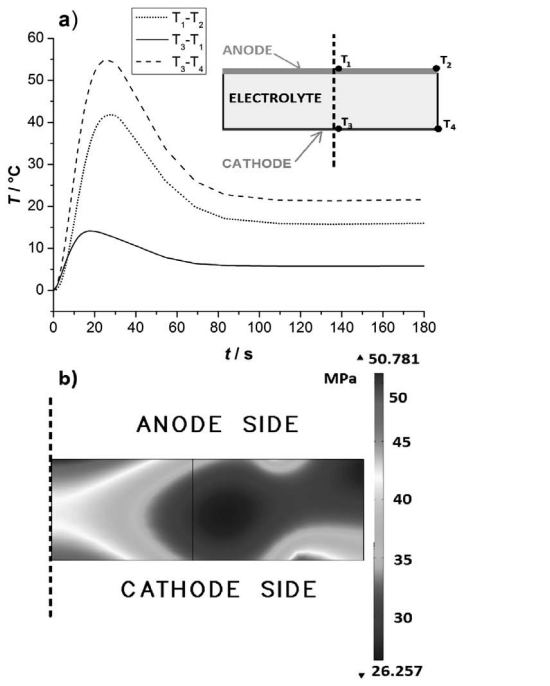


**Figure 4:** a) Temperature gradients during membrane heating in different directions, presented in the cross-section of the heated membrane, the points where the temperatures were measured and b) the maximum thermally induced stress during membrane heating (only one half of the membrane cross-section is presented)

**Slika 4:** a) Temperaturni gradienti v različnih smereh membrane med njenim segrevanjem; položaji točk, med katerimi se je merila temperaturna razlika in b) toplotno inducirane napetosti med segrevanjem membrane (prikazana je le polovica membrane)

phase boundary and lowest in the SDC electrolyte (< 1 MPa) quite distant from the phase boundary. The induced stress in the electrolyte increases when approaching the phase boundary, reaching its peak at the phase boundary, ≈ 9 MPa (the small insert in **Figure 3**). The nature of the shrinkage of both layers suggests that the stress at the cooled-down state is always tensile in the anode layer, while the electrolyte layer is under compression. Considering the fact that the compressive strength of SDC is much higher than the tensile strength of Ni-SDC (≈ 1 GPa and ≈ 150 MPa, respectively)[30], it would be expected that the Ni-SDC anode layer represents the weak point of the bilayer system where any potential cracking should occur. However, the adopted mathematical model revealed that the maximum tensile stress built in the anode layer never exceeds the Ni-SDC tensile strength. Such a prediction is in line with the practical observations, according to which no cracks are formed after the first thermal cycle (sintering and reduction).

A short testing cycle of the SOFC membranes requires rapid heating and cooling of the system. As already mentioned, a rapid temperature change may be a cause of crack formation and represents a decisive phase for the survival of a multilayer system. Cracks always appear as a consequence of various stresses. In the investigated case, there are two origins of the induced stresses: various expansions of the elements due to different thermal-expansion coefficients and thermal gradients across the membrane due to the unequal distances of both surfaces from the heating elements. Several temperature gradients in various directions may be defined in a cross-section of the heated membrane (**Figure 4a**). Furthermore, the temperature gradients vary as the membrane is heated up. At the maximum heating power (72 W for each plug) the induced temperature gradients reach their peaks after ≈ 28 s. With regards to the anode side, two important consequences may be drawn from the above facts. Raising the temperatures from the cooled-down state (≈ 25 °C) to the operating conditions (≈ 535 °C) will expand the anode Ni-SDC layer more than the electrolyte SDC layer. Thus, any given temperature above the cooled-down state causes some interlayer relaxation, reducing the tensile stress in the anode layer. Additionally, the anode layer is relatively thin, meaning that across such a thin layer rather small temperature gradients may be induced during heating. According to the mathematical simulation, the overall residual stress in the anode layer is more influenced by the stress relaxation due to the thermal expansion than the induced thermal stress. Such a conclusion implies that the anode layer may not be a potential weak point of the tested multilayer system.

After conducting a similar investigation on the electrolyte layer, somewhat different conclusions may be drawn. When compared with the anode, the electrolyte layer is much thicker. In a relatively thick electrolyte layer, any accumulation of stress due to different thermal expansions of various layers is less pronounced and the major contribution to the overall stress comes from the thermally induced stress due to temperature gradients. The stress is dynamically changed in accordance with the altered temperature. There are two hot zones in the electrolyte: the outer surface and the anode/electrolyte phase boundary. Due to the induced thermal gradients, the adjacent electrolyte layer expands differently, thereby creating stress (**Figure 4b**). The adopted mathematical model predicts that the maximum stress in the electrolyte layer is built up near the anode/electrolyte phase boundary. In this region, the fact that not only the thermally induced stress plays an important role but so also do some minor contributions of the stress due to the adjacent anode layer is recognized. The absolute value of the induced maximum stress after ≈ 28 s (the time of the maximum temperature gradient across the membrane) is ≈ 50 MPa. This value practically reaches the tensile strength of SDC, which is 53 MPa.[28] When the maximum tensile strength is reached, the material is prone to cracking.

To verify the findings regarding the thermally induced stress, a SEM investigation was conducted on two cross-sections, i.e., on the multilayer system of the Ni-SDC anode, SDC electrolyte and Pt cathode after sintering and reduction in the cooled state and on the

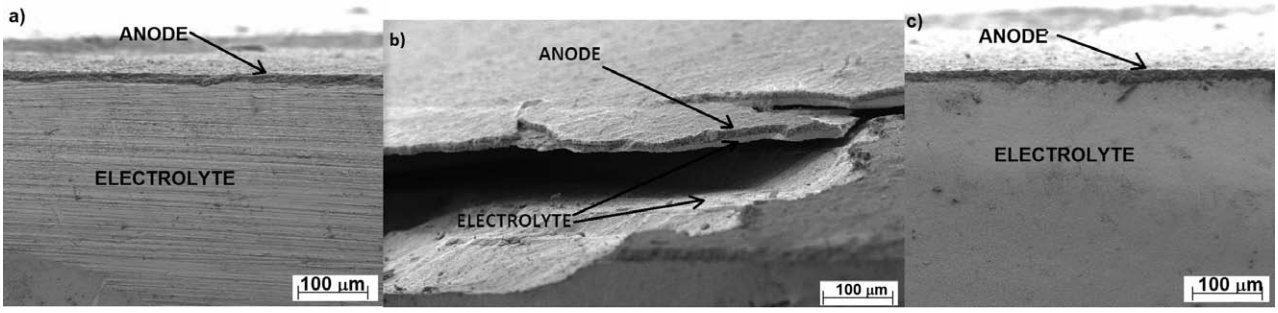


**Figure 5:** SEM micrographs of bilayer system Ni/SDC-SDC taken in the cooled state: a) after sintering and reduction, b) the same system after being additionally exposed to the maximum heating rate and c) the system heated with the optimum heating rate/thermal load
**Slika 5:** SEM-posnetki dvoplastnega sistema Ni/SDC-SDC v ohlajenem stanju: a) po sintranju in redukciji, b) isti sistem po dodatni izpostavitvi največji hitrosti ogrevanja in c) po segrevanju z optimalno hitrostjo glede na toplotno obremenitev

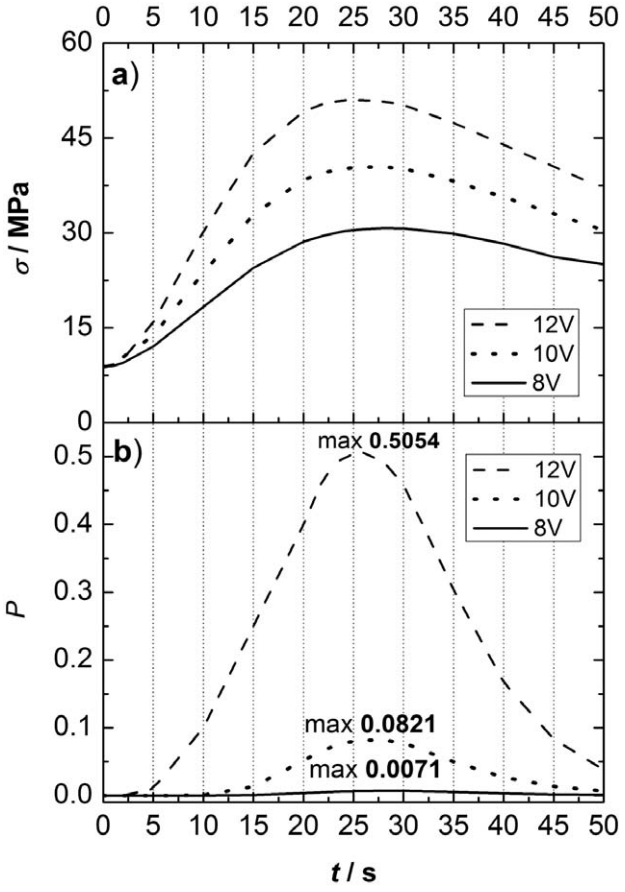


**Figure 6:** a) Induced tensile stress in the electrolyte layer (at the phase boundary) during heating with various thermal loads, b) failure probability of multilayer membrane Ni-SDC/SDC/Pt vs. time for various heating powers

**Slika 6:** a) Inducirane natezne napetosti v plasti elektrolita (na fazni meji) v odvisnosti od časa segrevanja pri različnih toplotnih obremenitvah in b) verjetnost odpovedi večplastne membrane Ni-SDC/SDC/Pt v odvisnosti od časa pri različnih močeh ogrevanja

same system after being additionally exposed to various heating rates (**Figures 5a** to **5c**). Particular focus was given to the anode-electrolyte phase boundary, since the appearance of cracks is most likely to occur immediately next to the boundary in the electrolyte where the tensile stress is maximum. As predicted by the mathematical model, the membrane survives the sintering and the subsequent reduction cycles without any crack formation. In contrast, when an identical membrane undergoes an additional heating cycle with the maximum heating rate, cracks appear. The mathematical model correctly predicts the crack formation in the electrolyte layer adjacent to the phase boundary. Crack propagation is parallel to the boundary, which is again in accordance with the mathematical model, in which the thermally induced tensile stress essentially changes layer by layer from one membrane surface to another.

Since rapid membrane heating induces the overcritical tensile stress in the electrolyte layer, the next logical task addresses the maximum tolerable heating rate without a detrimental effect for the membrane. This question was approached by conducting a series of mathematical modelling, in which the induced tensile stress in the electrolyte layer (at the phase boundary) versus the time was calculated (**Figure 6a**). It appears that the induced stress may be substantially lowered by reducing the heating power of the heat plugs. Operating at 83.3 % of the maximum heating power ($W/W_{max}$) reduces the maximum induced stress in the electrolyte layer to 35 MPa, thereby considerably increasing the chances of membrane survival (**Figure 5c**). This finding is very important since it substantially reduces the number of experiments required for determining the initial operating conditions and thus saves a great deal of time.

The failure of a SOFC membrane (or a stack) is most often caused by the brittle nature of the ceramic materials.[31] From the previous section, it is evident that in the investigated system the electrolyte is the most susceptible to fraction. It is, therefore, valuable to analyse the failure probability of the electrolyte for the purpose of improving the reliability of the membrane. The measured values of the characteristic mechanical properties for the SOFC multilayer system generally correspond to the Weibull distribution, particularly for brittle ceramic materials. The failure probability $P$ of brittle ceramic materials is often modelled with the following equation:

$$P = 1 - \exp\left[\left(-\frac{\sigma}{\sigma_0}\right)^m\right] \quad (11)$$

where $\sigma$, $\sigma_0$ and $m$ are the induced thermal stress, the characteristic tensile strength and the 2-parametric Weibull parameter, respectively.[20] According to the above modelling, the weak point of the investigated system is in the electrolyte layer during the membrane heating. Thus, the tensile strength and the Weibull parameter of SDC are 53 MPa and 9.09, respectively.[28] With this model (Eq. 11), the failure probability ($P$) was calculated (**Figure 6b**). The maximum failure probability always occurs at the maximum induced stress. It is evident that at the maximum heating power $W_{max}$, the failure probability reaches 50.54 %. This rather high $P$ value is impractical even during laboratory testing and completely unacceptable for any practical application. However, the $P$ value can be lowered by reducing the $W/W_{max}$ ratio. If the $W/W_{max}$ ratio is lowered to 83.3 %, the $P$ value does not exceed 8.21 %, making such testing conditions fairly acceptable for laboratory development. A failure probability of not more than 0.71 % is predicted if the $W/W_{max}$ ratio is further lowered to 66.7 %. With such a value $P$ dependence on the $W/W_{max}$ ratio it could be argued that the only acceptable heating rate for the investigated system should be a very low one. In other words, a rather low heating rate neglects the main advantage of the developed SOFC testing system, i.e., quick assembly or dismantling, and short testing cycles. However, as predicted by the mathematical model, a

lower $W/W_{max}$ ratio (for reaching a low $P$ value) is necessary only during the early stage of membrane heating. After several tens of seconds, the $W/W_{max}$ ratio can be increased even to the maximum value without a severe risk of a membrane failure.

## 4 CONCLUSION

A new SOFC testing system allowing quick testing cycles has been developed. The system's operation may be successfully described with finite-element modelling. The critical point with respect to the membrane failure was recognized during the early stage of the system heating. The maximum thermally induced stress during the heating was found in the electrolyte layer adjacent to the anode/electrolyte phase boundary. The absolute value of the induced maximum stress was close to the tensile strength of the SDC, causing some crack formation. To reduce the probability of a membrane failure, the heating power of the testing system should be lowered only during the early stage of the membrane heating. Afterwards, it can be increased to its maximum value without a severe risk of a membrane failure.

## 5 REFERENCES


[1] S. M. Hail, Acta Mater, 51 (**2003**), 5981–6000

[2] F. Tietz, I. Arul Raj, W. Jungen, D. Stöver, Acta Mater, 49 (**2001**), 803–810

[3] T. Suzuki, Z. Hasan, Y. Funahashi, T. Yamaguchi, Y. Fujishiro, M. Awano, Science Magazine, 325 (**2009**), 852–855

[4] Y. Yin, S. Li, C. Xia, G. Meng, Electrochimica Acta, 51 (**2006**), 2594–2598

[5] A. B. Stambouli, E. Traversa, Renew. Sustain. Energ. Rev., 6 (**2006**), 433

[6] J. Li, T. Ikegami, T. Mori, Acta Mater, 52 (**2004**), 2221–2228

[7] J. Wright, A. Virkar, J. Power Sources, 196 (**2011**), 6118–6124

[8] M. Chen, B. H. Kim, Q. Xu, B. K. Ahn, W. J. Kang, D. P. Huang, Ceram. Inter., 35 (**2009**), 1335–1343

[9] M. Chen, B. H. Kim, Q. Xu, O. J. Nam, J. H. Ko, J. Eur. Ceram. Soc., 28 (**2008**), 2947–2953

[10] W. Jung, H. Park, Y. Kang, D. Yoon, Ceram. Int., 36 (**2010**), 371–374

[11] Q. Liu, X. Dong, C. Yang, S. Ma, F. Chen, J. Power Sources, 195 (**2010**), 1543–1550

[12] X. Fang, G. Zhu, C. Xia, X. Liu, G. Meng, Solid state ionics, 168 (**2004**), 31–36

[13] Y. Yin, W. Zhu, C. Xia, G. Meng, J. Power Sources, 132 (**2004**), 36–41

[14] C. M. Grgicak, R. G. Green, W. F. Du, J. B. Giorgi, J. Am. Ceram. Soc., 88 (**2005**), 3081–3087

[15] H. Yakabe, Y. Baba, T. Sakurai, M. Satoh, I. Hirosawa, Y. Yoda, J. Power Sources, 131 (**2004**), 278–284

[16] W. Fischer, J. Malzbender, G. Blass, R. W. Steinbrech, J. Power Sources, 150 (**2005**), 73–77

[17] C. R. He, W. G. Wang, J. Wang, Y. Xue, J. Power Sources, 196 (**2011**), 7639–7644

[18] K. P. Recknagle, R. E. Williford, L. A. Chick, D. R. Rector, M. A. Khaleel, J. Power Sources, 113 (**2003**), 109–114

[19] L. Petruzzi, S. Cocchi, F. Fineschi, J. Power Sources, 118 (**2003**), 96–107

[20] M. Ambrožič, K. Vidovič, Mater. Tehnol., 41 (**2007**) 4, 179–184

[21] O. C. Zienkiewicz, R. Taylor, The Finite Element Method: Volumes 1, 2 & 3, 5th ed., Elsevier, Butterworth–Heinemann, 2000

[22] J. N. Reddy, An Introduction to the Finite Element Method, McGraw-Hill, 1993

[23] K. J. Bathe, Finite Element Procedures, Prentice Hall, Englewood Cliffs, New Jersey 1996

[24] A. Selimovic, M. Kemm, T. Torisson, M. Assadi, J. Power Sources, 145 (**2005**), 463–469

[25] C. K. Lin, T. T. Chen, Y. P. Chyou, L. K. Chiang, J. Power Sources, 164 (**2007**), 238–251

[26] T. Skalar, A. Golobič, M. Marinšek, J. Maček, Mater. Tehnol., 47 (**2013**) 4, 423–429

[27] T. Skalar, J. Maček, A. Golobič, J. Eur. Ceram. Soc., 32 (**2012**), 2333–2339

[28] S. Sameshima, T. Ichikawa, M. Kawaminami, Y. Hirata, Mater. Chem. Phys., 61 (**1999**), 31–35

[29] T. Zhang, Q. Zhu, W. L. Xie, X. Xin, J. Power Sources, 182 (**2008**), 540–545

[30] X. B. Li, H. Y. Wang, H. X. Gu, J. Wang, W. J. Zhang, T. G. Wang, Sci. Sinter., 42 (**2010**), 153–159

[31] W. Yanli, K. L. Duncan, E. D. Wachsman, F. Ebrahimi, J. Am. Ceram. Soc., 90 (**2007**), 3908–3914